Far-infrared sensor for cirrus (FIRSC): an aircraft-based Fourier-transform spectrometer to measure cloud radiance

Michael D. Vanek, Ira G. Nolt, Nina D. Tappan, Peter A. R. Ade, Fred C. Gannaway, Peter A. Hamilton, Clare Lee, Jesse E. Davis, and Steve Predko

We describe an aircraft-based Fourier-transform spectrometer (FTS) designed to measure the Earth outgoing radiance spectrum in the far-infrared–submillimeter spectral range. The instrument features include a rapid-scan FTS to obtain high spatial resolution from a moving aircraft platform, a sensitive two-channel detector, and a CCD camera for recording the nadir cloud scene with each scan record. Such measurements demonstrate the sensitivity of Earth radiance to high clouds and provide spectral data for improving techniques for remote sensing and retrieval of atmospheric and cloud properties.

OCIS codes: 300.6270, 280.1310.

1. Introduction

The lack of a global cirrus cloud database is a major deficiency in the experimental validation of general circulation models that are the basis for estimating long-term climate change. Theoretical models for the retrieval of ice cloud (cirrus) properties from submillimeter–microwave radiance spectra are a recent development.[1,2] The far-infrared–submillimeter spectral region (100 μm < wavelength < 1000 μm) is optimally suited for cirrus cloud observations, since at these wavelengths ice particles are relatively transparent but scatter strongly. Submillimeter wavelengths are comparable with the sizes of cirrus ice particles, and thus scattering is in the Mie regime. As a result the scattering-induced temperature depression in the outgoing Earth radiance is highly sensitive to integrated ice mass (ice water path) and particle size but relatively insensitive to cloud temperature. Fourier-transform spectroscopy (FTS) is the logical choice for the spectral study of cirrus radiance. FTS can provide a wide spectral range to resolve ice particle size and at the same time sufficient spectral resolution for marginal resolution of upper tropospheric line features. For frequencies less than 100 cm^{-1} tropospheric pressure-broadened line widths are typically <0.1 cm^{-1}. Furthermore, by use of a polarizing FTS in a slant-path viewing mode, particle shape or habit information can be inferred from the difference in the vertical and the horizontal linear polarization components of the radiance.[2]

Our objective in this study was to design a FTS aircraft instrument to measure the Earth spectral radiance. The most difficult requirement was for a spectral noise-equivalent temperature sensitivity (NEΔT) of order 1 K within a scan time of a few seconds. The short scan time is necessary to resolve cloud spatial structure to better than 1 km at the typical airspeeds of a jet aircraft. To achieve this sensitivity in the submillimeter band below 70 cm^{-1}, we employed a composite bolometric detector cooled to 0.3 K and for the frequency band above 80 cm^{-1} a Ge:Ga photodetector at 4.2 K. The main emphasis in the instrument design was to achieve high sensitivity in the atmospheric windows between 10 and 40 cm^{-1} where scattering by typical ice clouds has the largest effects in terms of the Earth brightness temperature.

2. Far-Infrared Sensor for Cirrus

The far-infrared sensor for cirrus (FIRSC) was configured as a Martin–Puplett polarizing interferome-

M. D. Vanek (m.d.vanek@larc.nasa.gov), I. G. Nolt, and N. D. Tappan are with NASA Langley, Hampton, Virginia 23681. P. A. R. Ade, F. C. Gannaway, P. A. Hamilton, and C. Lee are with Queen Mary and Westfield College, London E1 4NS, UK. K. F. Evans is with the University of Colorado, Boulder, Colorado 80309. J. E. Davis is with Cochise Instruments, Hereford, Arizona 85615. S. Predko is with the University of Oregon, Eugene, Oregon 97403.
Received 15 May 2000; revised manuscript received 16 October 2000.
0003-6935/01/132169-08$15.00/0

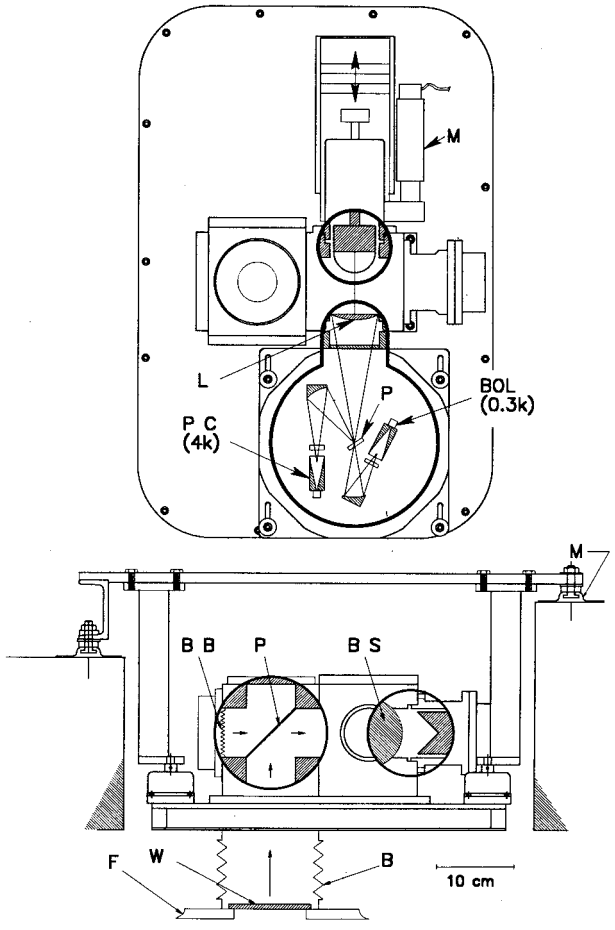

Fig. 1. Top and end views of FIRSC. M, mirror; L, lens; BOL, bolometer; P, polarizer; BS, beam splitter, F, fuselage; W, window.

ter and built in a collaborative program between NASA and several university groups. In a Martin–Puplett configuration, dihedral (rooftop) mirrors replace the usual flat mirrors of a Michelson interferometer and a linear polarizing grid is the beam splitter. The instrument can operate in an intensity- or a polarization-sensing mode.[3] The cryogenic detector system was designed by Queen Mary and Westfield College on the basis of a similar system developed for the European SAFIRE-Airborne program.[4]

The Martin–Puplett configuration provides two separate input and output ports defined by reflection/transmission from input and output polarizer elements. Figure 1 shows cross-sectional views of the optical configuration. The instrument attaches to the plane floor and views the upwelling cloud radiance through a nadir-viewing 4-mm-thick polyethylene window (W) installed in the fuselage. The input polarizer (P) combines one polarization component of the nadir radiance with an orthogonal component from the reference blackbody (BB) as input to the beam splitter (BS), which has a polarization axis rotated by 45° relative to the input polarizer. The input to the beam splitter will be elliptically polarized by any difference in sky-reference intensities. The beam splitter divides the incident beam into two orthogonally polarized components, one transmitted to a fixed mirror arm and the other to a moving mirror. The fixed and the moving dihedral mirrors act to rotate the plane of polarization by 90° upon reflection in each arm. Thus the initially transmitted component is reflected upon its return to the beam splitter and vice versa for the other arm. The recombined beam will be elliptically polarized but with the direction of its major axis a function of the phase difference resulting from the path difference. As a result an output polarizer with an axis 45° relative to the beam splitter provides reflected/transmitted power, which is modulated in an interferometric sense by the scene-BB source difference. The detectors sense equal and opposite modulations. For example, at zero path difference the difference in intensity will be positive on one detector and negative on the other. With matched detectors this complementary modulation can be used differentially to eliminate common mode noise.[5] In our case the two channels are independently optimized to span different spectral ranges.

In Fig. 1 the fixed-arm and 5.4-cm-diameter dihedral mirror is seen in cross-section in the lower view and the movable one in the top view. The output polarizer is placed in the Dewar at the focus of the $f/3.5$ condensing lens (L). The polarizer provides two output ports that are separately optimized to span two ranges between 10 and 140 cm^{-1}. The lower range is sensed by a bolometer (BOL) cooled to 0.3 K, and the range above 80 cm^{-1} with an unstressed Ge:Ga photoconductor (PC) at 4.2 K. The usable high-frequency response of the present instrument is limited to $\sim$150 cm^{-1} by the rolloff in polarizing efficiency of the free-standing wire-grid beam splitter. Tests of photolithographic beam splitters to improve the polarization efficiency at higher frequencies have not been successful, owing to the acoustic-induced vibration in flight. The detector and preamplifier systems are discussed in more detail in Section 4. To reduce the absorption by water vapor, the instrument is purged in flight by the boiloff N_2 and He_2 gas ($\sim$2 l/min) from the detector cryostat. The dry gas flow, after its passage through the interferometer, is vented to a Mylar-covered camera window to keep it free of frost.

The temperature-controlled BB in the horizontally viewing input port defines the reference or zero signal level in the measured spectrum. For sky radiance data the BB reference was maintained at 25 $\pm$ 0.5 °C. For in-flight calibration a shutter-type ambient temperature BB is inserted into the nadir port. Calibration spectra are then recorded with the reference BB in the other port at 25 and 65 °C. In this configuration the measured spectral output is the intensity difference (65–25 °C) between the two BBs. This measurement calibrates the spectral radiance responsivity for the radiance interior to the fuselage polyethylene window. The variance of repeated calibration spectra defines the noise-equivalent delta temperature (NEΔT) for a specified scan time and spectral resolution. Corrections for the window

Table 1. Measurement and Instrument Parameters

Parameter	FIRSC
Channel 1	10–70 cm^{-1} (1998) 10–35 cm^{-1} (1999)
Channel 2	80–135 cm^{-1}
Spectral Resolution	0.10 cm^{-1} (unapod)
Field of View	0.03 rad
Footprint	<1 km
Input aperture	5.4-cm diameter
Scan time	4 s
Max opt. path diff.	±5 cm
Max mirror stroke	±2.5 cm
Mirror scan vel.	1.25 cm/s
Signal frequency	2.5 Hz/cm^{-1}
Detectors	
Channel 1	Bolometer @ 0.3 K
Channel 2	Ge:Ga PC @ 4.2 K
Bolometer NEΔT (10–35 cm^{-1})	1-K rms at 30 cm^{-1} varying as freq^{-2}
Photoconductor NEΔT (90–130 cm^{-1})	1.2-K rms

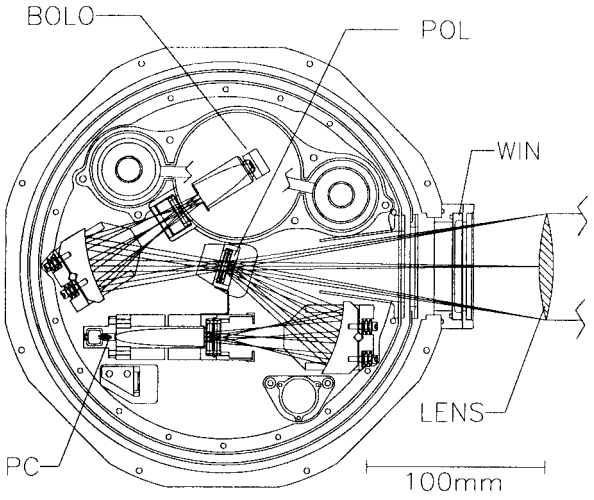

Fig. 2. This figure shows the layout of optics on the 4.2-K cold plate of the cryostat. The field of view is defined by a 5-mm aperture at the polarizer (POL). The transmitted and the reflected components are reimaged to the bandpass filters and parabolic feedhorns and to integrating cavities containing the detector.

transmission are incorporated into the NEΔT instrument precision values. The typical data system settings for double-sided interferogram scan parameters are summarized in Table 1.

Instrument control and data acquisition are performed with a compact PCI Pentium-based computer with LabView software. Each channel is sampled with triggering by the drive encoder at 4-μm increments (ten encoder pulses) for a total of 12,500 values per scan for each channel. This sampling is approximately 4 times Nyquist for the highest spectral frequency of 150 cm^{-1}. The data are recorded on a removable optical disk. Initial engineering flights were made in 1998 with the NASA Wallops T-39 (Sabreliner) and in 1999 with a commercially leased Lear 25C operated by Flight International Corporation.[6]

3. Signal Modulation Considerations

The instrument operates in rapid scanning mode. In principle, rapid scanning can provide twice the performance of chopper-modulated phase-sensitive detection.[7,8] This reflects the fact that in rapid scanning the instrument is integrating the source signal all the time, the only modulation being the cosine modulation as a function of path difference. However, rapid scanning constrains the detector bandwidth to be matched to the audio-frequency spectrum of the modulated spectral band. The PC detector is inherently fast under high-photon background and has a measured frequency response of ~3 kHz. With a bolometric detector there is a trade-off between the detector time constant, τ, and sensitivity, which is dependent on the thermal conductance to the heat reservoir, G. The requirement to be photon noise limited essentially fixes G, and the response speed is determined from $\tau = C/G$, where C is the heat capacity of the bolometer and G the thermal conductance to the heat sink. A bolometer temperature of 0.3 K is necessary to provide a sufficiently reduced heat capacity for the required detector bandwidth. For the 1998 flights with a spectral high-frequency filter cutoff of 65 cm^{-1}, the detector response bandwidth was 240 Hz. In 1999 the spectral bandwith was lowered to 35 cm^{-1}, and the reduced optical loading and detector temperature resulted in a bolometer bandwidth of 500 Hz. The time constants for both channels provide nearly optimum filter efficiency for the nominal scan parameters. In the case of the bolometer, which integrates as a resistor–capacitor (RC) filter, the calculated filter efficiency is >0.96.[7,8] The laboratory bandwidth measurements are in excellent agreement with the bolometer time constants observed for the heat pulses caused by cosmic ray particles incident on the bolometer. High-energy cosmic particles produced signal spikes in flight at a frequency of ~1/min, which reflects the cosmic particle flux intercepted by the 3-mm-diameter bolometer substrate aligned in the vertical plane.[9] On the ground cosmic-particle-generated pulses are relatively rare, owing to the greater shielding by the atmosphere.

4. Detector System

The optical elements of the detector are cooled to 4.2 K in an IR Labs HD-8 cryostat with a cold baseplate diameter of 200 mm. Figure 2 shows the optical and detector layout, and Fig. 3 is a photo viewing along the direction of the entering beam. The 300-mK bolometer temperature is achieved by use of a closed-cycle dual-stage ^{4}He–^{3}He refrigerator.[5,10] The polarizer (POL) is at the focus of the lens located at the interferometer output, and its aperture of 5 mm at the focal distance of 180 mm defines the instantaneous field of view for the instrument. From the polarizer the reflected and the transmitted polarized

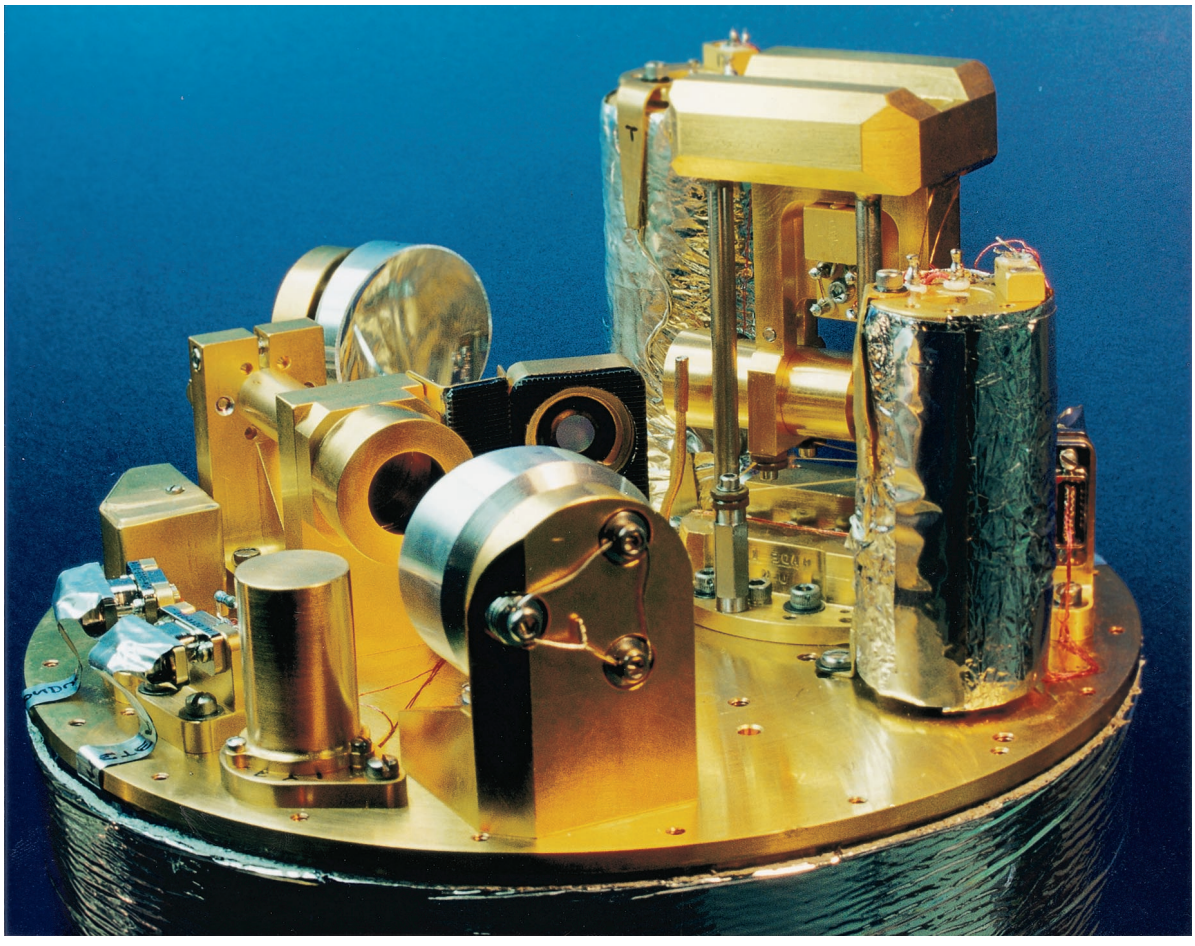

Fig. 3. Photo of the cryostat cold optics and detectors mounted to the 4.2-K cold plate. The $f/3.5$ beam from the interferometer entering from the lower right focuses at the 5-mm aperture of the output polarizer at the center of the cold plate. From here the aluminum off-axis mirrors reimage the transmitted and the reflected beams to the bolometer and PC detectors, respectively. In the left foreground are the radiation enclosures for the warm dual-JFET and TIA preamplifiers and the lowpass filter (black) at the input to the PC detector feedhorn. In the background the bolometer feedhorn is seen suspended from the double-chambered ^{4}He–^{3}He stage. The cylindrical elements are the ^{3}He and ^{4}He adsorption pumps.

signal components are reimaged to the apertures of the feedhorns that hold the final bandpass-limiting filters. To minimize common-mode microphonic and electromagnetic interference pickup in the severe aircraft environment, both detectors employ balanced preamplifier input stages by use of cold junction field effect transistors (JFETs). The resulting preamplifier outputs are carried in a fully differential manner to the analog-to-digital (A–D) interface. The PC JFET is an InterFET INF146, and the bolometer transimpedance amplifier (TIA) JFET is an IR Labs module containing a monolithic dual-silicon JFET and heater. A Dewar-attached battery-powered amplifier conditions the cold preamp outputs further before being interfaced to the data-acquisition A–D interface. The amplifier gain is typically 100 for the bolometer and unity for the PC detector. Similar bolometer detector electronics are described in more detail in Naylor *et al.*[5]

The bolometer is a composite element consisting of a small (≈0.5-mm) Ge:Ga crystal with a large temperature coefficient of resistance bonded to a 3-mm diameter by 30-μm-thick sapphire substrate. A 100-nm-thick bismuth film on the substrate provides the impedance to maximize the absorption of radiation. The sensor for the higher-frequency channel is an extrinsic bandgap Ge:Ga photoconductor giving a spectral response edge at 80 cm^{-1}. Table 2 summarizes the detector parameters. In this table electrical noise-equivalent power (NEP) refers to power absorbed in the detector, whereas optical NEP refers to response for an external BB source. The signal-to-noise ratio has a broad maximum around the optimum bias current of 250 nA.

5. Data-Acquisition System

The instrument is controlled by a Pentium CPU Compact PCI-based computer consisting of the processor board, SCSI disk controller, multiaxis motor controller for the moving mirror linear drive motor and for a stepper-motor scan mirror drive to rotate between the in-flight calibration sources and the nadir scene, a global positioning system receiver, a multichannel 16-bit A–D converter board, and a digital image cap-

Table 2. Detector Parameters

Parameter	Bolometer		Photoconductor
	0–35-cm^{-1} Bandpass	0–70-cm^{-1} Bandpass	80–135-cm^{-1} Bandpass
Temp (K)	0.28	0.31	4.2
Time constant (ms)	0.32	0.62	$<$0.05
Bandwidth (Hz)	500	240	3000
Resistance (MΩ)	4.0	0.5	$\approx$3
Responsivity (MV/W)	2.0	2.5	25
Noise (nV/√Hz) for $\upsilon >$10 Hz	10	17	800
Electrical NEP (W/√Hz) ($\times 10^{-14}$)	0.5	0.7	3
Optical NEP (W/√Hz) ($\times 10^{-14}$)	1.1	4.6	36

ture board. The data are recorded on an optical disk. The system control software is implemented with LabView.

Each detector is sampled by a drive controller triggering at 4-μm drive increments (=10 encoder pulses and 8 μm in optical path difference) providing $> 4\times$ Nyquist for the highest spectral response frequency of 150 cm^{-1}. A typical flight of 2 h accumulates approximately 0.5 Gbyte of data about equally divided between the interferogram and TIF format scene image data. Global positioning system time, position, and track data are also recorded in the scan header format.

6. Measured Spectra and Calibration

The system NEΔT was measured with the same BB calibration configuration in the laboratory and in flight at 41,000-ft altitude. For calibration a BB at ambient measured temperature is moved into the sky port between the polyethylene aircraft window and the bottom port to the interferometer. Scans are obtained for the reference BB at controlled temperatures of 25 and 65 °C. The rms variation of repeated scans (lower trace in Fig. 4) defines NEΔT for a single 4-s scan. For the bolometer channel the single-scan NEΔT equals 1.2 K at 30 cm^{-1} and varies inversely with frequency squared. This is the same noise level as measured in the laboratory environment and shows the effective suppression of aircraft microphonic and electromagnetic interference noise by the differential TIA amplifier design. Since the calibration target is located inside the fuselage window, the calibration refers to the radiance at the input to the interferometer interior to the window. Future modifications for higher-altitude operation will install the instrument in an unpressurized instrument pod without the need for a pressure window. Figure 4 shows the calibration reproducibility on three flights with a reference-calibration temperature difference of 48 °C.

Figure 5 shows examples of upwelling radiance as seen through the fuselage polyethylene window for different cloud conditions from an altitude of 41,000 ft. For these two cases, balloon radiosondes indicated similar temperature profiles. The main difference was deep diffuse cirrus between 6 and 12 km in the case of Flight 13 (F13) with ground details visible from aircraft altitude implying a cirrus visible optical depth of 1–2. The effect of cirrus scattering is seen to reduce the sky brightness consistently with scat-

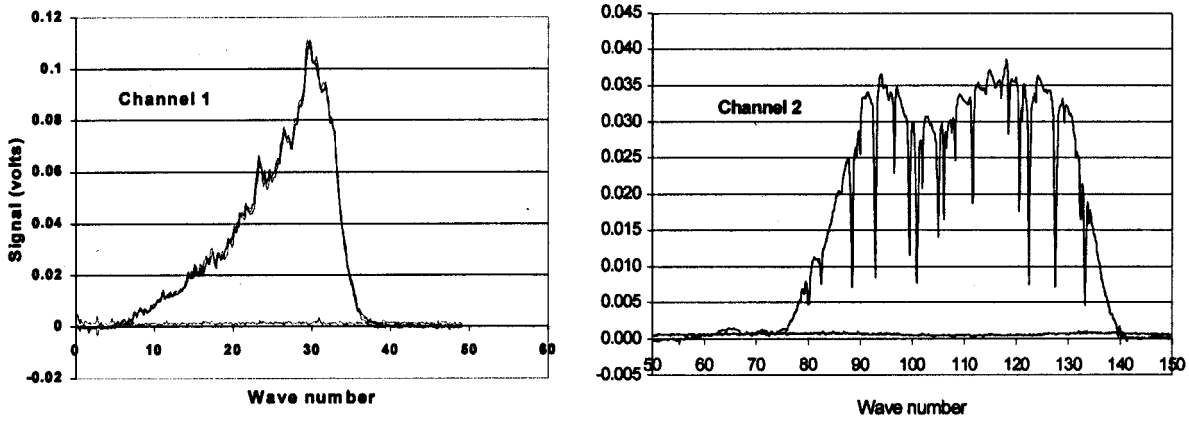

Fig. 4. Examples of inflight calibrations for a nadir port BB temperature 48 °C lower than the reference port BB for the two spectral bands as operated in the 1999 flights. The left panel shows the reproducibility for the bolometer channel of three in-flight calibrations on different flights. Each flight calibration is the average of ten 4-s scans in which the lower trace is the standard deviation for a 4-s scan based on the variation within a sample of ten single scans. Channel 1 shows the approximate frequency-squared dependence of the Planck function for the source difference. In channel 2 dry gas purging does not eliminate absorptions by water vapor in the instrument path.

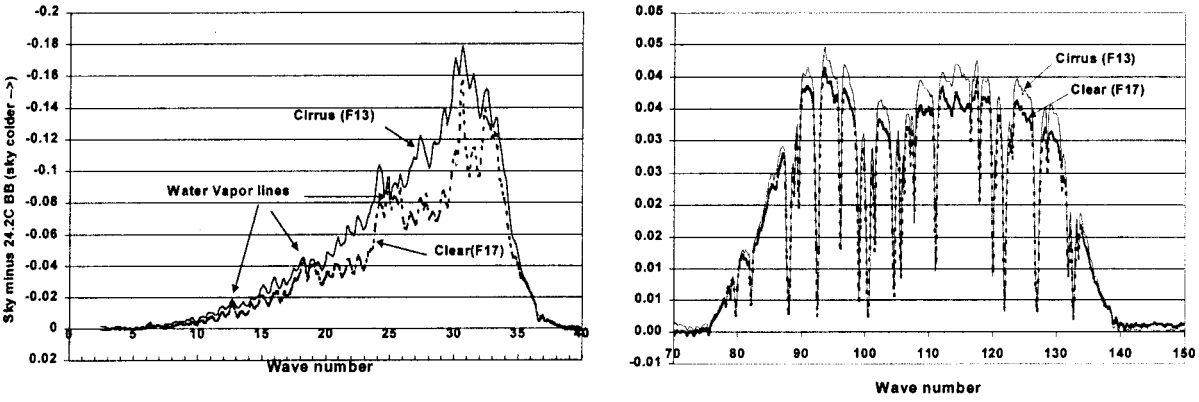

Fig. 5. Measured spectra averaged over 8 km (ten scans) from 41,000-ft altitude for clear and for cirrus conditions. The measured signal is the difference of the sky minus the reference BB with reversed polarity for channel 2. The regions of strong water line absorption saturate in a short distance and are insensitive to cloud conditions. The periodic channel fringes seen in channel 1 with a 0.8-cm^{-1} spacing result from the 4-mm-thick polyethylene fuselage window.

tering models except where affected by strong water-vapor absorption lines.[1,2] With the calibration measurement the measured spectra can be converted to brightness temperature. The calibration of channel 2 is complicated by strong water absorption and window emissivity effects and we have not, as yet, achieved a satisfactory absolute calibration model for this channel. These window effects will be eliminated in the conversion under way for the instrument to operate in an unpressurized instrument pod, thus simplifying the spectral calibration. We have modeled the calibration for channel 1 where the window absorption and emission effects are relatively small and the cirrus effects maximum. In this channel the window thickness is of the order of a few wavelengths, and the channel fringing can be modeled as a low finesse Fabry–Perot cavity.[11] The resulting window transmission and reflection terms, τ_{win} and r_{win}, respectively, can then be used, along with knowledge of the window temperature, to generate a spectral correction for the window. The equation for the instrument viewing the calibration source is

$$V_{cal\_spectra} = \Gamma(\tau_{bb}\epsilon_{bb}T_{bb} - \tau_{ref}\epsilon_{bb}T_{ref}), \quad (1)$$

where τ_{bb} and τ_{ref} are the transmissions of the two input ports, T_{bb} is the second port reference BB temperature, and T_{ref} is the temperature of the calibration source inserted into the scene port.

When the terms are rearranged, the instrument calibration constant (scale factor) becomes

$$\Gamma = V_{cal\_spectra}/(\tau_{bb}\epsilon_{bb}T_{bb} - \tau_{ref}\epsilon_{bb}T_{ref}). \quad (2)$$

The equation for the calibrated measured spectra viewed through the fuselage window is

$$V_{meas\_spectra} = \Gamma\{T_{bb} - \tau_{ref}[(\tau_{win} - r_{win})T_{scene} + \epsilon_{win}T_{win} + (r_{win}\epsilon_{inst})T_{inst}]\}. \quad (3)$$

When the terms are rearranged, the calibrated spectra in terms of absolute scene temperature becomes

$$T_{scene} = [1/t_{ref}(t_{win} - r_{win})]\{T_{bb} - [(1/\Gamma)(V_{meas\_spectra}) + t_{ref}e_{win}T_{win} + t_{ref}r_{win}\epsilon_{inst}T_{inst}]\}. \quad (4)$$

The calibrated results for the data in Fig. 5 are shown in Fig. 6. The effect of the window is to reduce the apparent sky brightness by ~10 K, and the resulting window correction has an uncertainty of ±1.5 K, mainly because of the uncertainty in the window temperature. Table 3 lists the random and the systematic uncertainties.

The largest systematic uncertainty is the absolute emissivity of the reference BB. The BB is composed of carbon-loaded Epotek epoxy with an inverted pyramidal surface with a groove depth of 1.5 mm.[12] Spectral reflectance measurements show an emissivity above 10 cm^{-1} of better than 0.99 ± 0.01. These factors plus the instrument precision combine for an

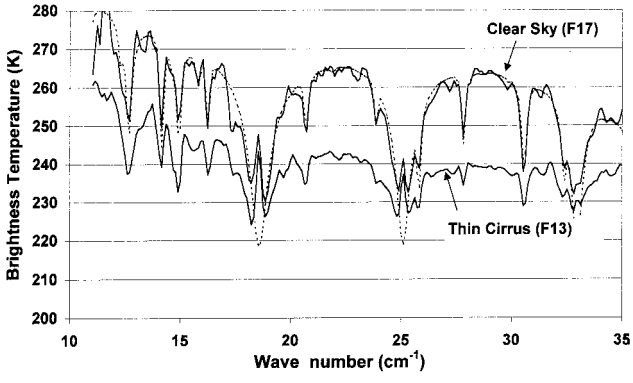

Fig. 6. Comparison of similarly calibrated cirrus and clear-sky radiance for the measured spectra in Fig. 5. The largest reductions in brightness temperature occur in atmospheric window regions. The center portions of the strong water lines at 18.6 and 25 cm^{-1} are affected by residual water vapor within the instrument. The dashed curve is the clear-sky brightness calculated for a line-by-line atmospheric model using coincident radiosonde temperature and humidity data.

Table 3. Random and Systematic Uncertainty Components

	Magnitude (K)	Source	Uncertainty (1σ)
Precision	±2.0	Spectral noise (NEΔT)	±1.2 K at 30 cm^{-1} varying inversely with frequency
		Window correction	±1.5 K
		BB temp	±0.5 K
Systematic	3	BB emissivity ($\epsilon = 0.99 \pm 0.01$)	3 K

absolute calibration uncertainty of ±4 K. In Fig. 6 clear-sky radiance is compared with that calculated with an atmospheric line-by-line radiative-transfer model and radiosonde-measured temperature and humidity profiles. The agreement is good except for the centers of the strong water lines, which are affected by water-vapor emission within the instrument, and for a feature or artifact on the low-frequency wing of the 18.6-cm^{-1} water line. For the data in Fig. 6, the cirrus was marginally transparent, consistent with brightness temperature depressions of 20 ± 2 K in the windows at 22 and 30 cm^{-1}, where the uncertainty in the difference of the ten scan average spectra is mainly due to the window correction. The reader is referred to the research of Evans *et al.*[1,2] for a description of the scattering properties of cirrus at far-infrared wavelengths.

7. Polarization Measurement

The theory for cirrus scattering predicts a difference in radiance between the horizontally (*H*) and vertically (*V*) polarized radiance components when viewed at a slant angle. This difference arises in part from the preferential horizontal orientation of the major axis for nonspherical particles.[2] To measure polarization, a mirror was mounted external to the fuselage window viewing 70° from the nadir direction and with the instrument polarizations aligned to *H* and *V* axes. In this mode the input polarizer is replaced with a mirror. For a measurement of cirrus polarization a flight track including a reverse track was made over variable cirrus including a short visibly clear area. The resulting measurement of the $V - H$ brightness at 30 cm^{-1} is shown in Fig. 7. The polarization difference varied from zero to a maximum in correspondence with the visual appearance of cirrus. Shortly after reversal of the track, the input polarizer was reinstalled for obtaining brightness temperature data corresponding to the *H* polarization brightness.

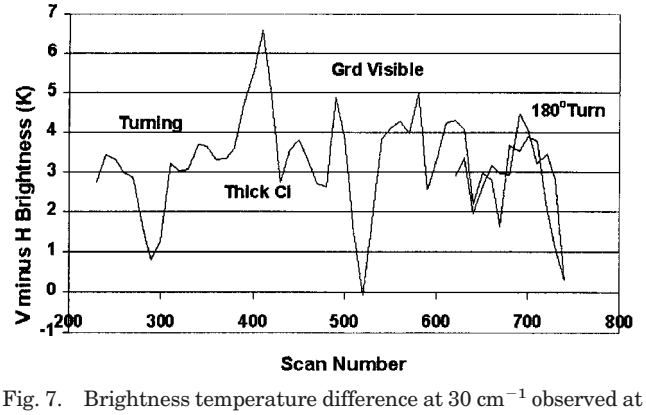

Fig. 7. Brightness temperature difference at 30 cm^{-1} observed at a view angle of 70° from nadir. Each measurement point is an average of ten single scans and has a NEΔT of ≈0.3 K. Zero polarization difference was observed over the visibly clear segment.

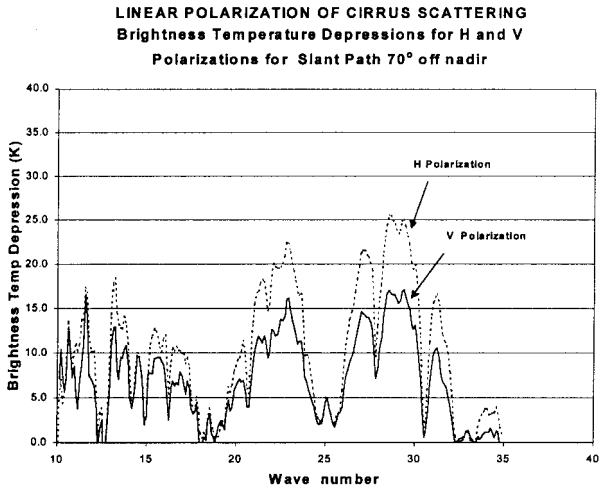

Fig. 8. Temperature depression for *H* and *V* linear polarization observed 70° from nadir.

The spectral variation of the largest measured polarization (near scan 400 in Fig. 7) is shown in Fig. 8. This was obtained by means of applying the spectral $V - H$ brightness difference relative to the difference in *H* absolute brightness between the clear sky and the cirrus scans. Averages of 12 spectra (1 min or 10 km along track) for cirrus and clear segments were subtracted to generate the *H* polarization temperature depression spectrum by the cirrus. From this result the *V* temperature depression is inferred by subtraction of the $V - H$ spectrum measured in the other instrument mode in the same general location.

8. Conclusions

In this paper we have described the design and performance of a polarizing Fourier-transform spectrometer for use in aircraft-based studies of the cloud-modulated Earth radiance. Combined with an advanced detector system technology, the results demonstrate the spectral properties of Earth radiance with unprecedented sensitivity, spectral, and spatial resolution. This instrument technology is closely related to, and benefits from, related applications in astronomy. Balanced differential signal electronics is shown to eliminate the usual in-flight degradation in performance from a noisy aircraft environment. Good agreement is found with the abso-

lute calibration and atmospheric model calculations based on coincident radiosonde temperature and relative humidity measurements.

The correction for channel fringing and emission of the fuselage pressure window is the largest uncertainty in the absolute calibration of brightness temperature. This window calibration uncertainty will be eliminated when the instrument is adapted for operation in an unpressurized instrument pod attached to a high-altitude aircraft such as the Proteus or the ER-2.

The authors acknowledge the cooperation and enthusiasm of many participants. We thank the NASA Wallops Flight Facility and Flight International, Inc., for their excellent flight support; David Naylor of the University of Lethbridge and B. Bach of Hyperfine Inc. for optical component fabrication; Jennifer Alltop for help with data analysis; and Peter Hargrave for the detector photograph. Financial support for this program was provided by Langley Director's Discretionary grants in 1998–1999 and by the NASA Earth Science Enterprise and Earth Science Technology Offices.

References and Note

1. K. F. Evans, A. H. Evans, I. G. Nolt, and B. T. Marshall, "The prospect for remote sensing of cirrus clouds with a submillimeter-wave spectrometer," J. Appl. Meteor. **38,** 514–525 (1999).
2. K. F Evans, S. J. Walter, A. J. Heymsfield, and M. N. Deeter, "Modeling of submillimeter passive remote sensing of cirrus clouds," J. Appl. Meteor. **37,** 184–205 (1998).
3. D. H. Martin and E. Puplett, "Polarization interferometric spectrometer for millimeter and submillimeter spectroscopy," Infrared Phys. **10,** 105–109 (1969).
4. P. Dickinson, B. Carli, P. A. R. Ade, I. Nolt, J. Leotin, and M. Carlotti, "SAFIRE-A an airborne far infra-red limb sounder," in *Global Process Monitoring and Remote Sensing of the Ocean and Sea Ice*, D. W. Deering and P. Gudmandsen, eds., Proc. SPIE **2586,** 214–224 (1995).
5. D. A. Naylor, B. G. Gom, P. A. R. Ade, and J. E. Davis, "Design and performance of a dual polarizing detector system for broadband astronomical spectroscopy at submillimetre wavelengths," Rev. Sci. Instrum. **70,** 4097–4109 (1999).
6. Flight International, Inc., Special Projects Division, Patrick Henry Airport, Newport News, Va.
7. B. Carli and V. Natale, "Efficiency of spectrometers," Appl. Opt. **18,** 3954–3958 (1979).
8. B. Carli, F. Mencaraglia, and A. Bonetti, "Submillimeter high-resolution FT spectrometer for atmospheric studies," Appl. Opt. **23,** 2594–2603 (1984).
9. I. G. Nolt, J. V. Radostitz, M. Carlotti, B. Carli, F. Mencaraglia, and A. Bonetti, "Cosmic-ray backgrounds in infrared bolometers," Int. J. Infrared Millim. Waves **6,** 707–727 (1985).
10. Chase Research, 35 Wolstenholm Road, Sheffield S7 1LB, UK.
11. M. Born and E. Wolf, *Principles of Optics*, 6th ed. (Pergamon, New York, 1980), p. 323.
12. C. Lee, "Far infrared spectroscopic measurements of HBr in the lower stratosphere," Ph.D. dissertation (Queen Mary and Westfield College, London, 1997), p. 297.